Manipulating the magnetic energy density and energy flux by cylindrically symmetric state of polarization

Yuan, Wenfeng; Man, Zhongsheng

DOI
10.1016/j.ijleo.2019.03.103

Publication date
2019

Document Version
Final published version

Published in
Optik

Optik - International Journal for Light and Electron Optics 185 (2019) 208–214

Contents lists available at ScienceDirect

Optik

journal homepage: www.elsevier.com/locate/ijleo

Original research article

Manipulating the magnetic energy density and energy flux by cylindrically symmetric state of polarization

Wenfeng Yuan[a], Zhongsheng Man[a,b,*]

[a] School of Physics and Optoelectronic Engineering, Shandong University of Technology, Zibo 255049, China
[b] Optics Research Group, Delft University of Technology, Department of Imaging Physics, Lorentzweg 1, 2628CJ Delft, The Netherlands

ARTICLE INFO

Keywords:
Diffractive optics
Polarization
Optical tweezers or optical manipulation

ABSTRACT

Using the Richards and Wolf formulas for an arbitrary cylindrical vector (CV) beam, we obtain explicit expressions for all components of the electric and magnetic field strength vectors near the focus, as well as expression for the energy flux in an aplanatic optical system. Based on such analytical models, it reveals that the intensity pattern of the magnetic field at the focus can be tailored by appropriately adjusting the initial phase, peak-centered, doughnut, and flat-topped magnetic fields can be achieved using this method. For the energy flows, in contrast, they are almost the same for arbitrary CV beams, which exhibit hollow shaped patterns for both the transverse and longitudinal components. Unlike the longitudinal component, however, the hollow shaped pattern of the transverse component is separated into two regions, arriving from the null transverse energy flow in the focal plane. Besides, the directions of the transverse energy flow are reversed between these two regions, which are directed inwardly and outwardly along the radial direction, respectively.

1. Introduction

Cylindrical vector (CV) optical fields, due to the unique polarization and focusing properties, have attracted a great deal of attention and interest [1]. Two important members of CV beams are radially polarized (RP) and azimuthally polarized (AM) beams. It has been demonstrated that a RP beam can be focused by a high numerical aperture (NA) objective lens to generate a strong longitudinally polarized electric field near focus [2–4]. While for an AP beam, it can be used to achieve a hollow-shaped electric field with pure azimuthal polarization [2–4]. Besides, more fruitful polarization and intensity profiles have also been successfully demonstrated for the electric field near the focal region when considering the additional amplitude and phase modulations, including sharper focus [5–9], multiple focal spots [10–13], optical needle [14–17], flat-top focus [4,18], optical chain [19,20], focal spot array [21–25], optical channel [26–28], optical cage [29–31], and spherical spot [32–35]. These peculiar properties are useful for many potential and practical applications such as optical trapping and manipulation of particles [36,37], high resolution microscopy [38], optical data storage [39], electron acceleration [40]. Moreover, the localized spin angular momentum of RP [41] and AP [42] beams are demonstrated, and arbitrary spin-orientated and super-resolved focal spot are achieved by the superposition of a RP and AP beams [43]. For all the above cases, the studies are mainly focused on the focal behaviors of electric field. As a counterpart, the attempts to target magnetic field shaping as well as energy flux of the CV beams in the aplanatic system have not yet been pursued.

In this paper, we study the magnetic field distributions and energy flux near the focus of the strongly focused CV beams. Using the Richards and Wolf method for arbitrary CV beams, we obtain explicit expressions for all components of the electric and magnetic field

* Corresponding author at: School of Physics and Optoelectronic Engineering, Shandong University of Technology, Zibo 255049, China.
E-mail address: zsman@sdut.edu.cn (Z. Man).

https://doi.org/10.1016/j.ijleo.2019.03.103
Received 1 February 2019; Accepted 19 March 2019

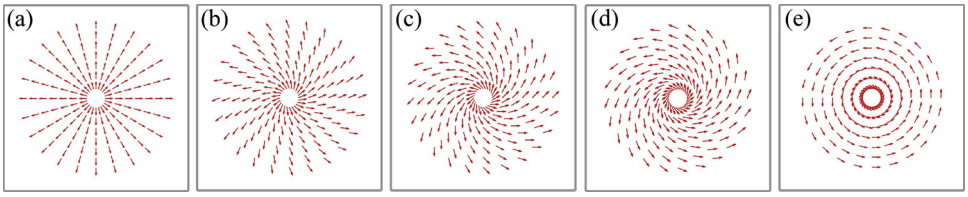

Fig. 1. Polarization distributions of five kinds of CV beams with ϕ_0 = (a) 0, (b) π/8, (c) π/4, (d) 3π/8, and (d) π/2, respectively.

strength vectors near the focus, as well as the energy flux of an aplanatic optical system. Based on such analytical models, it is found that the intensity pattern of the focal magnetic field highly depends on the initial phase, peak-centered, doughnut, and flat-topped magnetic fields can be obtained using this method. For the energy flows, in contrast, they are almost the same for arbitrary CV beams and exhibit hollow shaped patterns for both the transverse and longitudinal components. Unlike the longitudinal component, however, the hollow shaped pattern of the transverse component is separated into two regions, arriving from the null transverse energy flow in the focal plane. Furthermore, the directions of the transverse energy flow are reversed between these two regions, which are directed inwardly and outwardly along the radial direction, respectively.

2. Theory

For any given polarized beam, its state of polarization (SoP) could be mathematically described by the combination of a pair of orthogonal base vectors. When referring to the generalized CV beam, it can be denoted as follows [1]

$$\begin{aligned}\mathbf{E}_0 &= \tfrac{A_0}{\sqrt{2}}\{\exp[i(\varphi+\varphi_0)]\mathbf{e}_r + \exp[-i(\varphi+\varphi_0)]\mathbf{e}_l\}\\ &= A_0[\cos(\varphi+\varphi_0)\mathbf{e}_x + \sin(\varphi+\varphi_0)\mathbf{e}_y],\end{aligned} \tag{1}$$

where A_0 is a constant, ϕ is the azimuthal angle, ϕ_0 is the initial phase, $\mathbf{e}_r$ and $\mathbf{e}_l$ represent, respectively, the unit vectors of right-handed and left-handed circular polarization, $\mathbf{e}_x$ and $\mathbf{e}_y$ are unite vectors of linear polarization along x and y axis, respectively.

Obviously, the SoP described by Eq. (1) only depends on the azimuthal angle ϕ, thus its local SoPs are variant only in the azimuthal direction. Further, the two components in term of horizontal and vertical polarizations are always in phase, hence the local SoPs are all linearly polarized, as can be seen in Fig. 1, which depicts the polarization distributions of five kinds of CV beams with $\phi_0 = 0, \pi/8, \pi/4, 3\pi/8, \pi/2$. For $\phi_0 = 0$ and $\pi/2$, they represent, respectively, RP and AP beams, which are two extreme cases of CV beams. For other values of ϕ_0, they are generalized CV beams. The electric and magnetic fields of strongly focused optical field can be calculated using the Richards and Wolf method [44]. When the incident optical field is denoted by Eq. (1), the corresponding three-dimensional electric and magnetic fields near focus can be derived in cylindrical coordinate system (r, φ, z) as [44]

$$\begin{bmatrix}\mathbf{E}(r,\ \phi,\ z)\\ \mathbf{H}(r,\ \phi,\ z)\end{bmatrix} = \frac{-ikf}{2\pi}\int_0^{2\pi}\int_0^{\alpha}\sqrt{\cos\theta}\,l(\theta)\sin\theta\begin{bmatrix}\mathbf{M}_E\\ \mathbf{M}_H\end{bmatrix}\exp(i\boldsymbol{k}_0\cdot\boldsymbol{r})\mathrm{d}\varphi\mathrm{d}\theta. \tag{2}$$

Here, the wavenumber $k = 2\pi/\lambda$, where λ is the wavelength in free space; f is the focal length of the focusing objective lens; the maximum tangential angle $\alpha = \arcsin(\mathrm{NA}/n)$, where NA and n are the numerical aperture and the refractive index in the image space that we take as 0.95 and 1, respectively;θ and ϕ denote, respectively, the tangential angle with respect to z axis and the azimuthal angle with respect to x axis; $\mathbf{M}_E$ and $\mathbf{M}_H$ represent the propagating electric and magnetic polarization vectors in the image space; $\boldsymbol{k}_0 = (-\sin\theta\cos\phi,\ -\sin\theta\sin\phi,\ \cos\theta)$ is the unite vector of the wave vector; $\boldsymbol{r} = (r\cos\varphi, r\sin\varphi, z)$ is the polar vector of arbitrary point in the image space; $l(\theta)$ is the relative amplitude of the input optical field at the entrance pupil plane, which we consider the Bessel-Gaussian beam that given by [2]

$$l(\theta) = \exp\left[-\beta^2\left(\frac{\sin\theta}{\sin\alpha}\right)^2\right]J_1\left(2\beta\frac{\sin\theta}{\sin\alpha}\right), \tag{3}$$

where β is the ratio of the pupil radius and the beam waist, which we take as 1 in our configuration; and J_1 is the first-order Bessel function of kind one.

In Eq. (2), the electric and magnetic polarization vectors in terms of $\mathbf{M}_E$ and $\mathbf{M}_H$ can be respectively derived as

$$\mathbf{M}_E = \begin{bmatrix}\mathrm{M}_E^x\\ \mathrm{M}_E^y\\ \mathrm{M}_E^z\end{bmatrix} = \begin{bmatrix}-\sin\varphi_0\sin\varphi + \cos\varphi_0\cos\theta\cos\varphi\\ \sin\varphi_0\cos\varphi + \cos\varphi_0\cos\theta\sin\varphi\\ \cos\varphi_0\sin\theta\end{bmatrix}, \tag{4}$$

$$\mathbf{M}_H = \sqrt{\frac{\varepsilon}{\mu}}\begin{bmatrix}\mathrm{M}_H^x\\ \mathrm{M}_H^y\\ \mathrm{M}_H^z\end{bmatrix} = \sqrt{\frac{\varepsilon}{\mu}}\begin{bmatrix}-\cos\varphi_0\sin\varphi - \sin\varphi_0\cos\theta\cos\varphi\\ \cos\varphi_0\cos\varphi - \sin\varphi_0\cos\theta\sin\varphi\\ -\sin\varphi_0\sin\theta\end{bmatrix}, \tag{5}$$

where, ε and μ denote the dielectric constant and the magnetic permeability of the image space. Apparently, the distributions of the

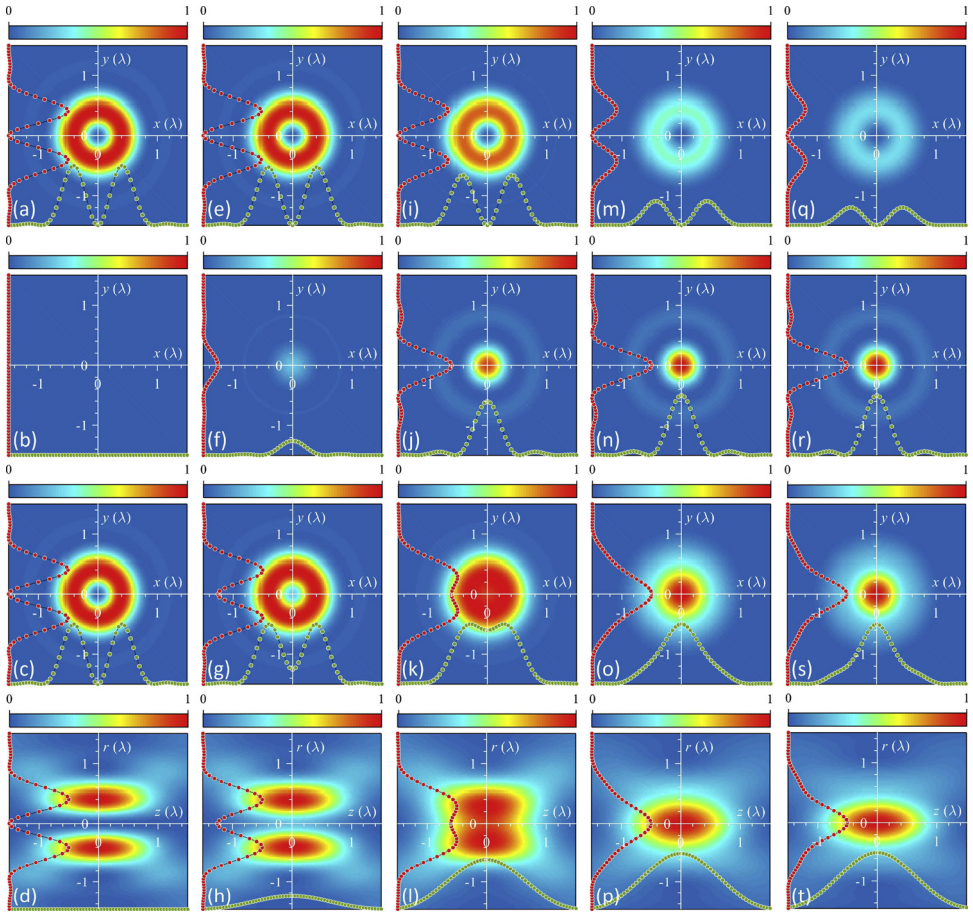

Fig. 2. Calculated magnetic field intensity distributions in the focal and through-focus planes of five kinds of CV beams with $\phi_0 = 0$, $\pi/8$, $\pi/4$, $3\pi/8$, and $\pi/2$ (columns 1–5, respectively). The transverse, longitudinal, and total fields in the focal plane are shown in the first, second, and third row, respectively. The last row is total magnetic field intensity distribution in the through-focus plane. All the intensities are normalized to the maximum intensity near focus for each input beam mode. The intensity profiles along coordinate axises are also presented for each image.

magnetic polarization vector described in Eq. (5) is much different from that of the electric polarization vector denoted in Eq. (4). In terms of the three-dimensional electric and magnetic field vectors, the energy current can be defined by the time-averaged Poynting vector [44]:

$$\mathbf{P} \propto \frac{c}{8\pi} \mathrm{Re}\,(\mathbf{E}\times\mathbf{H}^*), \tag{6}$$

where the asterisk denotes complex conjugation. We can calculate the magnetic fields and energy flow in the focal region of strongly focused CP beams using Eqs. (2)–(6).

3. Results and discussion

We now investigate the magnetic field distributions in the focal region of the high-NA focusing system, which might be useful in magnetic resonance microscopy [45], magneto-optical data storage [46], atom trapping [47], and all-optical magnetic recording [48]. The calculated intensity distributions of the magnetic fields in the focal and through-focus planes of five kinds of CV beams with $\phi_0 = 0$, $\pi/8$, $\pi/4$, $3\pi/8$, and $\pi/2$ are presented as Fig. 2. As proved in Fig. 1, all these beams exhibit perfect rotationally symmetric polarization distributions. Therefore, their focal magnetic fields show good circularly symmetric intensity distributions in the focal plane depicted in the first three rows in Fig. 2. However, they are much different. To be specific, it is an on-axis energy null and annular intensity distribution for the total field [Fig. 2(c) and (d)] when $\phi_0 = 0$, which is totally contributed by the transverse component [Fig. 2(a)]. By the contrary, the on-axis hot spot plays the dominate role for the total field [Fig. 2(s) and (t)] when $\phi_0 = \pi/2$, which is mainly contributed by the longitudinal component [Fig. 2(r)]. Besides, we can see the on-axis field is primarily contributed by the longitudinal component, whereas the outer part of the field is contributed by the transverse component. Moreover, the longitudinal component grows greatly with an increase in ϕ_0, whereas the transverse component weakens.

The trend that the longitudinal component becomes stronger than the transverse component has been proved in Fig. 2. For giving

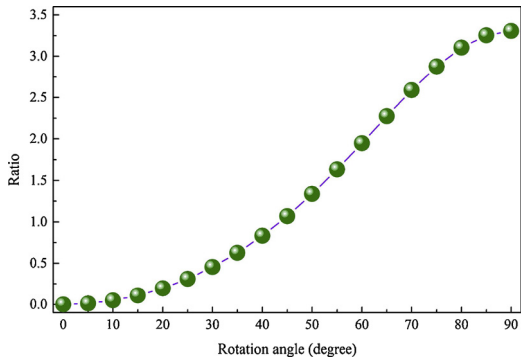

Fig. 3. Ratio of the maximum intensities of the longitudinal and transverse components versus the initial phase ϕ_0 when NA = 0.95.

a detailed and quantitative studies, Fig. 3 depicts the ratio of the maximum intensities of the longitudinal and transverse components versus the initial phase ϕ_0, which is 0, 0.0120, 0.0483, 0.1094, 0.1964, 0.3106, 0.4537, 0.6270, 0.8320, 1.0692, 1.3375, 1.6334, 1.9498, 2.2749, 2.5911, 2.8762, 3.1051, 3.2540, and 3.3057 for $180\phi_0/\pi = 0$, 5, 10, 15, 20, 25, 30, 35, 40, 45, 50, 55, 60, 65, 70, 75, 80, 85, and 90, respectively. Meanwhile, it is calculated to be about 43.61° for ϕ_0 when the maximum intensities of the transverse and longitudinal components are equal, as depicted in Fig. 4(a). Most importantly, a flat-topped magnetic field can be obtained by carefully tailoring the parameter ϕ_0, as shown in Fig. 4(b). Under this situation, the ratio of the maximum intensities of the longitudinal and transverse components is calculated to be about 1.3262, and ϕ_0 is approximately 49.80°.

The study of energy flow in the focal region of an aplanatic optical system has always attracted research interest [49–53] due to the potential applications like manipulating and transporting absorptive particles. In absorbing a certain portion of the beam energy, the absorptive particles simultaneously obtain the associated portion of its energy flow, which causes the motion of the particle with trajectory coinciding in direction with the Poynting vector. Fig. 5 shows the corresponding energy flow in the through-focus plane of the aforementioned CV beams in Fig. 1. The upper and lower rows display, respectively, the transverse and longitudinal components of the normalized Poynting vectors. Different from their focal magnetic field behaviors that are closely related to the initial phase ϕ_0, CV beams always generate nearly the same energy flows for both the transverse and longitudinal components. The longitudinal energy flow, which exhibits a hollow shaped pattern, is much stronger than that of the transverse one. Additionally, no transverse energy flows can be found in the focal plane ($z = 0$) and on axis ($r = 0$), they all located in the four quadrants and have a reversed direction before and after the focal plane.

For giving a deep understanding of energy flow, Fig. 6 shows the calculated Poynting vectors of aforementioned CV beams in the planes perpendicular to the optical axis. The first and second rows illustrate the transverse component of the normalized Poynting vector in the planes with $z = -0.5\lambda$ and 0.5λ, respectively. The last row depicts the longitudinal component of the normalized Poynting vector in the focal plane ($z = 0$). It is obvious that they all exhibit doughnut-shaped patterns. Interestingly, the transverse energy flows before and after the focal plane are both along the radial directions, but being directed inwardly and outwardly, respectively, which means the absorptive particles may be transported to the optical axis or away from it that is controlled by the location where the particles are trapped.

4. Conclusions

To summarize, we have proposed a simple method to manipulate the magnetic field and energy flow near the focus using CV

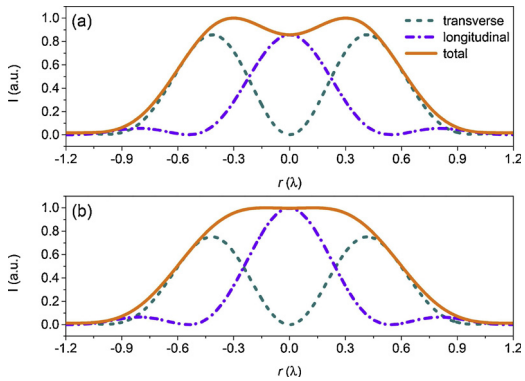

Fig. 4. Calculated magnetic field intensity profiles in the focal plane when (a) the ratio of the maximum intensities of the longitudinal and transverse components is equal and when (b) a flat-topped magnetic field is obtained.

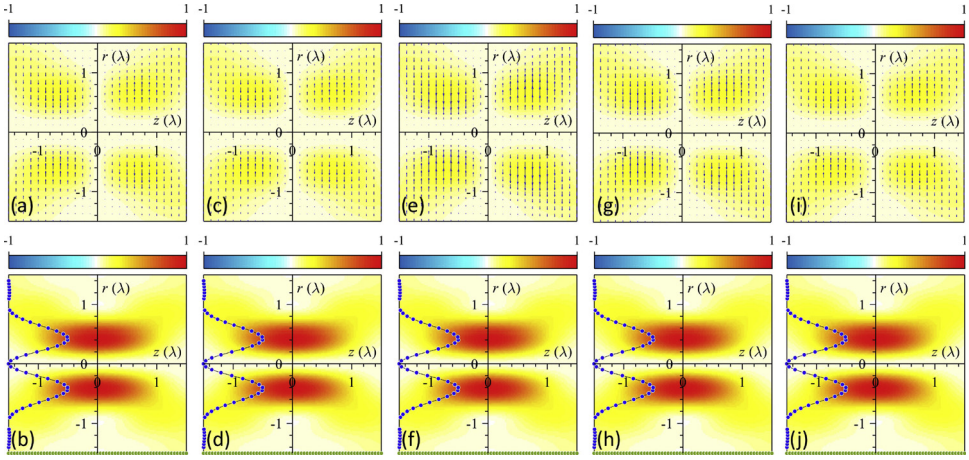

Fig. 5. Calculated Poynting vectors of the strongly focused CV beams with $\phi_0 = 0$, $\pi/8$, $\pi/4$, $3\pi/8$, and $\pi/2$, respectively. The upper and lower rows depict, respectively, the transverse and longitudinal components of the normalized Poynting vectors in the through-focus plane. The direction of the transverse energy flow is shown by the black arrows.

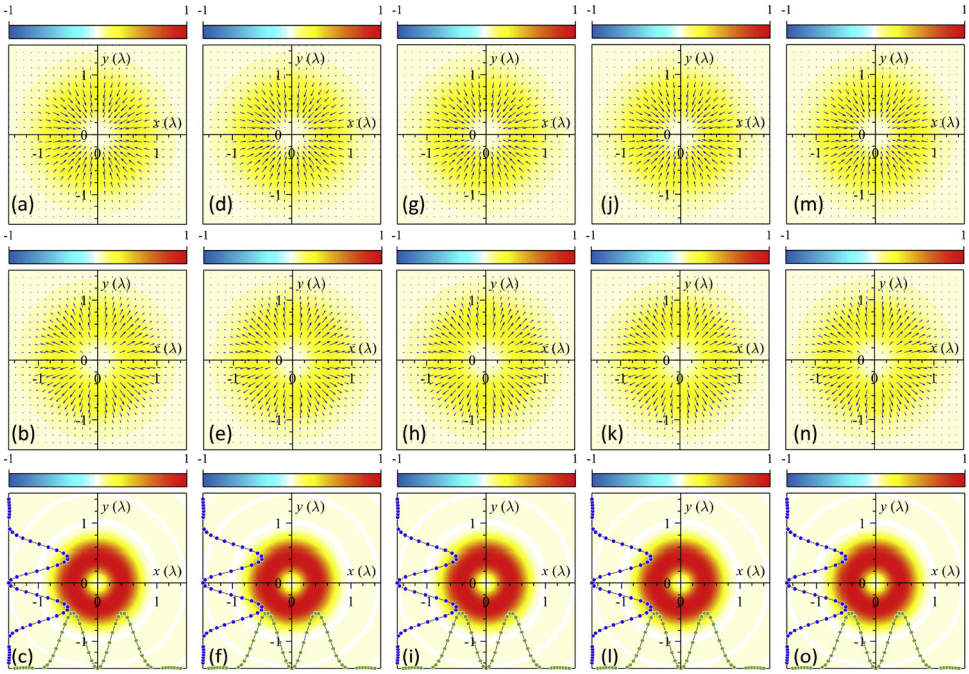

Fig. 6. Calculated Poynting vectors of the strongly focused CV beams with $\phi_0 = 0$, $\pi/8$, $\pi/4$, $3\pi/8$, and $\pi/2$, respectively. The first and second rows illustrate the transverse component of the normalized Poynting vector in the planes perpendicular to the optical axis with $z = -0.5\lambda$ and 0.5λ, respectively. The last row depicts the longitudinal component of the normalized Poynting vector in the focal plane ($z = 0$). The direction of the transverse energy flow is shown by the black arrows.

beams. Based on the Richards and Wolf method, we obtain explicit expressions for all components of the electric and magnetic field strength vectors near the focus, as well as the energy flux of arbitrary CV beams in an aplanatic optical system. Based on such analytical models, it is found that the intensity pattern of the focal magnetic field highly depends on the initial phase, peak-centered, doughnut, and flat-topped magnetic fields can be obtained by appropriately adjusting the initial phase. For the energy flows, in contrast, they are almost the same for arbitrary CV beams and exhibit hollow shaped patterns for both the transverse and longitudinal components. Unlike the longitudinal component, however, the hollow shaped pattern of the transverse component is separated into two regions, arriving from the null transverse energy flow in the focal plane. Further, the directions of the transverse energy flows are reversed between these two regions, which are directed inwardly and outwardly along the radial direction, respectively. Overall, the proposed method may be help in applications like magnetic recording, magnetic resonance microscopy, and optical micro-manipulation.

Acknowledgments

The work was supported by the National Natural Science Foundation of China under Grant No. 11604182, Natural Science Foundation of Shandong Province under Grant No. ZR2016AB05.

References

[1] Q. Zhan, Cylindrical vector beams: from mathematical concepts to applications, Adv. Opt. Photon. 1 (2009) 1–57.
[2] K.S. Youngworth, T.G. Brown, Focusing of high numerical aperture cylindrical vector beams, Opt. Express 7 (2000) 77–87.
[3] Z. Man, S. Fu, G. Wei, Focus engineering based on analytical formulae for tightly focused polarized beams with arbitrary geometric configurations of linear polarization, J. Opt. Soc. Am. A 34 (2017) 1384–1391.
[4] Q. Zhan, J.R. Leger, Focus shaping using cylindrical vector beams, Opt. Express 10 (2002) 324–331.
[5] R. Dorn, S. Quabis, G. Leuchs, Sharper focus for a radially polarized light beam, Phys. Rev. Lett. 91 (2003) 233901.
[6] Y. Kozawa, S. Sato, Sharper focal spot formed by higher-order radially polarized laser beams, J. Opt. Soc. Am. A 24 (2007) 1793–1798.
[7] G.Y. Chen, F. Song, H.T. Wang, Sharper focal spot generated by 4π tight focusing of higher-order Laguerre-Gaussian radially polarized beam, Opt. Lett. 38 (2013) 3937–3940.
[8] X. Hao, C. Kuang, T. Wang, X. Liu, Phase encoding for sharper focus of the azimuthally polarized beam, Opt. Lett. 35 (2010) 3928–3930.
[9] Z. Man, Z. Bai, S. Zhang, J. Li, X. Li, X. Ge, Y. Zhang, S. Fu, Focusing properties of arbitrary optical fields combing spiral phase and cylindrically symmetric state of polarization, J. Opt. Soc. Am. A 35 (2018) 1014–1020.
[10] H. Guo, X. Dong, X. Weng, G. Sui, N. Yang, S. Zhuang, Multifocus with small size, uniform intensity, and nearly circular symmetry, Opt. Lett. 36 (2011) 2200–2202.
[11] K. Huang, P. Shi, G.W. Cao, K. Li, X.B. Zhang, Y.P. Li, Vector-vortex Bessel-Gauss beams and their tightly focusing properties, Opt. Lett. 36 (2011) 888–890.
[12] M. Cai, C. Tu, H. Zhang, S. Qian, K. Lou, Y. Li, H.T. Wang, Subwavelength multiple focal spots produced by tight focusing the patterned vector optical field, Opt. Express 21 (2013) 31469–31482.
[13] P. Li, X. Guo, S. Qi, L. Han, Y. Zhang, S. Liu, Y. Li, J. Zhao, Creation of independently controllable multiple focal spots from segmented Pancharatnam-Berry phases, Sci. Rep. 8 (2018) 9831.
[14] H. Wang, L. Shi, B. Lukyanchuk, C. Sheppard, C.T. Chong, Creation of a needle of longitudinally polarized light in vacuum using binary optics, Nat. Photon. 2 (2008) 501–505.
[15] G.H. Yuan, S.B. Wei, X.C. Yuan, Nondiffracting transversally polarized beam, Opt. Lett. 36 (2011) 3479–3481.
[16] H. Dehez, A. April, M. Piché, Needles of longitudinally polarized light: guidelines for minimum spot size and tunable axial extent, Opt. Express 20 (2012) 14891–14905.
[17] Z. Man, C. Min, L. Du, Y. Zhang, S. Zhu, X. Yuan, Sub-wavelength sized transversely polarized optical needle with exceptionally suppressed side-lobes, Opt. Express 26 (2016) 874–882.
[18] X. Wang, B. Zhu, Y. Dong, S. Wang, Z. Zhu, F. Bo, X. Li, Generation of equilateral-polygon-like flat-top focus by tightly focusing radially polarized beams superposed with off-axis vortex arrays, Opt. Express 25 (2017) 26844–26852.
[19] Y. Zhao, Q. Zhan, Y. Zhang, Y.P. Li, Creation of a three-dimensional optical chain for controllable particle delivery, Opt. Lett. 30 (2005) 848–850.
[20] J. Wang, W. Chen, Q. Zhan, Creation of uniform three-dimensional optical chain through tight focusing of space-variant polarized beams, J. Opt. 14 (2012) 055004.
[21] H. Lin, B. Jia, M. Gu, Dynamic generation of Debye diffraction-limited multifocal arrays for direct laser printing nanofabrication, Opt. Lett. 36 (2011) 406–408.
[22] H. Lin, M. Gu, Creation of diffraction-limited non-Airy multifocal arrays using s spatially shifted vortex beam, Appl. Phys. Lett. 102 (2013) 084103.
[23] L. Zhu, J. Yu, D. Zhang, M. Sun, J. Chen, Multifocal spot array generated by fractional Talbot effect phase-only modulation, Opt. Express 22 (2014) 9798–9808.
[24] T. Zeng, C. Chang, Z. Chen, H.T. Wang, J. Ding, Three-dimensional vectorial multifocal arrays created by pseudo-period encoding, J. Opt. 20 (2018) 065605.
[25] J. Guan, N. Liu, C. Chen, X. Huang, J. Tan, J. Lin, P. Jin, Non-iterative dartboard phase filter for achieving multifocal arrays by cylindrical vector beams, Opt. Express 26 (2018) 24075–24088.
[26] B. Tian, J. Pu, Tight focusing of a double-ring-shaped, azimuthally polarized beam, Opt. Lett. 36 (2014) 2014–2016.
[27] J. Shu, Z. Chen, J. Pu, Y. Liu, Tight focusing of a double-ring-shaped, azimuthally polarized beam through a dielectric interface, J. Opt. Soc. Am. A 31 (2014) 1180–1185.
[28] L. Wei, H.P. Urbach, Shaping the focal field of radially/azimuthally polarized phase vortex with Zernike polynomials, J. Opt. 18 (2016) 065608.
[29] X. Weng, L. Du, P. Shi, X. Yuan, Creating adjustable uniform optical cages through polarization shaping in a low NA optical system, Appl. Opt. 56 (2017) 1046–1051.
[30] X. Weng, L. Du, P. Shi, X. Yuan, Tunable optical cage array generated by Dammann vector beam, Opt. Express 25 (2017) 9039–9048.
[31] Z. Man, Z. Bai, J. Li, S. Zhang, X. Li, Y. Zhang, X. Ge, S. Fu, Optical cage generated by azimuthal- and radial-variant vector beams, Appl. Opt. (2018) 3592–3597.
[32] N. Bokor, N. Davidson, Toward s spherical spot distribution with 4π focusing of radially polarized light, Opt. Lett. 29 (2004) 1968–1970.
[33] W. Chen, Q. Zhan, Creating a spherical focal spot with spatially modulated radial polarization in 4Pi microscopy, Opt. Lett. 34 (2009) 2444–2446.
[34] H. Lin, B. Jia, M. Gu, Generation of an axially super-resolved quasi-spherical focal spot using an amplitude-modulated radially polarized beam, Opt. Lett. 36 (2011) 2471–2473.
[35] S. Yan, B. Yao, R. Rupp, Shifting the spherical spot of a 4Pi focusing system, Opt. Express 19 (2011) 673–678.
[36] Y. Zhang, J. Wang, J. Shen, Z. Man, W. Shi, C. Min, G. Yuan, S. Zhu, H.P. Urbach, X. Yuan, Plasmonic hybridization induced trapping and manipulation of a sing Au nanowire on a metallic surface, Nano Lett. 14 (2014) 6430–6436.
[37] C. Min, Z. Shen, J. Shen, Y. Zhang, H. Fang, G. Yuan, L. Du, S. Zhu, T. Lei, X. Yuan, Focused plasmonic trapping of metallic particles, Nat. Commun. 4 (2013) 2891.
[38] Y. Kozawa, D. Matsunaga, S. Sato, Superresolution imaging via superscillation focusing of a radially polarized beam, Optica 5 (2018) 86–92.
[39] Y. Zhang, J. Bai, Improving the recording ability of a near-field optical storage system by higher-order radially polarized beams, Opt. Express 17 (2009) 3698–3706.
[40] J. Xu, Z.J. Yang, J.X. Li, W.P. Zang, Electron acceleration by a tightly focused cylindrical vector Gaussian beam, Laser Phys. Lett. 14 (2017) 025301.
[41] L. Han, S. Liu, P. Li, Y. Zhang, H. Cheng, J. Zhao, Catalystlike effect of orbital angular momentum on the conversion of transverse to three-dimensional spin states within tightly focused radially polarized beams, Phys. Rev. A 97 (2018) 053802.
[42] M. Li, Y. Cai, S. Yan, Y. Liang, P. Zhang, B. Yao, Orbital-induced localized spin angular momentum in strong focusing of optical vectorial vortex beams, Phys. Rev. A 97 (2018) 053842.
[43] W. Yan, Z. Nie, X. Liu, X. Zhang, Y. Wang, Y. Song, Arbitrarily spin-orientated and super-resolved focal spot, Opt. Lett. 43 (2018) 3826–3829.
[44] B. Richards, E. Wolf, Electromagnetic diffraction in optical systems II. Structure of the image field in an aplanatic system, Proc. R. Soc. London Ser. A 253 (1959) 358–379.
[45] M.S. Grinolds, M. Warner, K. De Greve, Y. Dovzhenko, L. Thiel, R.L. Walsworth, S. Hong, P. Maletinsky, A. Yacoby, Subnanometre resolution in three-dimensional magnetic resonance imaging of individual dark spins, Nat. Nanotechnol. 9 (2014) 279–284.
[46] P. Zijlstra, J.W.M. Chon, M. Gu, Five-dimensional optical recording mediated by surface plasmons in gold nanorods, Nature 459 (2009) 410–413.
[47] P. Schneeweiss, F. Le Kien, A. Rauschenbeutel, Nanofiber-based atom trap created by combining fictitious and real magnetic fields, New J. Phys. 16 (2014) 013014.

[48] A.R. Khorsand, M. Savoini, A. Kirilyuk, A.V. Kimel, A. Tsukamoto, A. Itoh, Th. Rasing, Role of magnetic circular dichroism in all-optical magnetic recording, Phys. Rev. Lett. 108 (2012) 127205.
[49] X. Jiao, S. Liu, Q. Wang, X. Gan, P. Li, J. Zhao, Redistributing energy flow and polarization of a focused azimuthally polarized beam with rotationally symmetric sector-shaped obstacles, Opt. Lett. 37 (2012) 1041–1043.
[50] X.Z. Gao, Y. Pan, G.L. Zhang, M.D. Zhao, Z.C. Ren, C.G. Tu, Y.N. Li, H.T. Wang, Redistributing the energy flow of tightly focused ellipticity-variant vector optical fields, Photon. Res. 5 (2017) 640–648.
[51] V.V. Kotlyar, A.A. Kovalev, A.G. Nalimov, Energy density and energy flux in the focus of an optical vortex: reverse flux of light energy, Opt. Lett. 43 (2018) 2921–2924.
[52] Z. Man, Z. Bai, S. Zhang, X. Li, J. Li, X. Ge, Y. Zhang, S. Fu, Redistribution the energy flow of a tightly focused radially polarized optical field by designing phase masks, Opt. Express 26 (2018) 23935–23944.
[53] S.N. Khonina, A.V. Ustinov, S.A. Degtyarev, Inverse energy flux of focused radially polarized optical beams, Phys. Rev. A 98 (2018) 043823.